Carbon 158 (2020) 146–156

Contents lists available at ScienceDirect

Carbon

journal homepage: www.elsevier.com/locate/carbon

Laser induced graphene fibers for multifunctional aramid fiber reinforced composite

Jalal Nasser [a], LoriAnne Groo [a], Lisha Zhang [b], Henry Sodano [a, b, c, *]

[a] Department of Aerospace Engineering, University of Michigan, Ann Arbor, MI, 48109, United States
[b] Department of Macromolecular Science and Engineering, University of Michigan, Ann Arbor, MI, 48109, United States
[c] Department of Materials Science and Engineering, University of Michigan, Ann Arbor, MI, 48109, United States

ARTICLE INFO

Article history:
Received 18 September 2019
Received in revised form
4 November 2019
Accepted 24 November 2019
Available online 25 November 2019

ABSTRACT

Aramid fiber reinforced composites have been limited to ballistic applications due to their poor structural performance, easy delamination, and their lack of multifunctionality. Given the poor adhesion of aramid fibers to polymeric matrices, the resulting composites suffer from weak interfacial and interlaminar properties. In this work, laser induced graphene (LIG) is formed directly on the surface of aramid fabrics with varying morphology to simultaneously improve the interlaminar strength of the composite and introduce multifunctionality. The LIG morphology is optimized for maximum improvement to the mechanical performance of the aramid fiber reinforced composite yielding a 70% and 20% increase in both short beam strength and Mode I fracture toughness, respectively. Remarkably, the improvement in interlaminar properties are reached while fully maintaining the specific strength and damping properties of the aramid fabric following the induction process. The improved interlaminar properties are attributed to the enhanced chemical interaction with the oxidized graphitic layer and mechanical interlocking across the interlaminar region due to the presence of the LIG. In addition, the LIG is shown to allow surface conductivity in aramid composites. This work shows that LIG can act as nanoscale building block in aramid fiber reinforced composites in order to provide a fast and cost-effective improvement to the mechanical performance and multifunctionality for structural applications.

1. Introduction

As fiber reinforced polymer matrix composites continue to replace conventional, homogeneous materials in a vast range of applications, the necessity to improve the design and multifunctionality of these materials is ever growing. A popular choice of fiber to use in such composites is *para*-phenylene terephthalamide (PPTA, or aramid), whose high specific strength and toughness, and low density provide it with excellent energy absorption [1]. These properties make aramid fiber reinforced polymer matrix composites ideal for ballistic and blast protection in applications such as hard body armor, rotor blades, engine nacelles and maritime vessels [2]. However, the high chemical stability of aramid fibers results in poor adhesion with polymer matrices, where the smooth and inert surface is unable to chemically react or mechanically interlock with the surrounding resin [3]. This results in considerable deviation between the actual properties of aramid fiber reinforced composites versus those expected based on the rule of mixtures, with inelastic deformation dominating the failure mode of the composites [2]. Therefore, the structural performance of these composites is noticeably inferior to that of carbon and glass fiber reinforced composites, thus restricting their potential application space [4]. Moreover, unlike carbon fibers, the electrically insulating nature of aramid fibers limits the design of multifunctional composites with embedded sensing [5], joule heating [6], damage detection [7,8], and lightning strike protection functions [9]. Therefore, it is necessary to design multifunctional aramid fiber reinforced composites with an improved structural performance for them to be integrated into a wider range of structural applications.

A number of reported methods and techniques aim to improve the mechanical performance of aramid fiber reinforced composites by strengthening the fiber-matrix interface. The enhancement of the interfacial properties of these composites is mainly achieved through an improvement of the chemical interaction or interfacial

---

* Corresponding author. Department of Aerospace Engineering, University of Michigan, Ann Arbor, MI, 48109, United States.
E-mail address: hsodano@umich.edu (H. Sodano).

https://doi.org/10.1016/j.carbon.2019.11.078

mechanical interlocking. By employing chemical treatments, the aramid surface can be populated with amino [10,11], hydroxyl [12,13], and carboxylic acid [14] functional groups that allow for improved chemical bonding with the resin. Such surface functionalization can be achieved through plasma treatment [15], acid or base hydrolysis [16,17], and ultra-sonication in resin baths [18,19]. However, many of these techniques cause surface defects and damage to the core of the aramid fiber, which reduces the tensile strength. For example, Benrashid et al. reported a 35% improvement of the interfacial shear strength (IFSS) of single aramid fiber epoxy matrix composites through a nitration process followed by a reduction of nitro groups into amino groups [20]. Yet these improvements came at the expense of the tensile properties of the fiber, with a decrease in strength of up 33% due to the surface damage caused by the harsh treatment conditions. Elsewhere, the grafting of specific moieties onto the fiber surface has been shown to improve the chemical interaction between the fiber and the matrix when performed under mild conditions [21]. However, the employed techniques are time-consuming and only compatible with specific resins, thus restricting its use in large scale industrial applications.

Another attractive interfacial reinforcement technique is the introduction of nanofillers into aramid fiber reinforced composites either through interphase design or by mixing them into the resin. When the nanomaterials are adhered to the aramid surface, such as in the case of ZnO nanoparticles [22], TiO_2 nanoparticles [23], and aramid fibrils [17], a larger and rougher surface area between the fiber and the matrix is created, thus improving interfacial mechanical interlocking. On the other hand, when large aspect ratio nanofillers, such as nanocellulose [24,25] and nanorods [26], are dispersed at low concentrations inside the liquid resin, the mechanical performance of the matrix is improved, thus enhancing the overall performance of the composite. Alternatively, aramid nanofibers (ANFs) have been introduced using various approaches into fiber reinforced composites in order to enhance their mechanical performance [27–29]. These nanofibers are obtained through a dissolution and deprotonation process that preserves the original chemical structure and increases the surface reactivity of the original fiber, thus making it highly compatible with aramid fibers [30]. Patterson et al. reported maximum improvements of 42% and 17% in short beam shear strength and Mode I fracture toughness, respectively, when ANFs were dispersed inside the epoxy matrix and infused into the aramid fabric [28]. The enhancement in interlaminar performance was attributed to the strengthening of the epoxy matrix, along with the chemical compatibility and hydrogen bonding between ANFs and the macroscale aramid surface. Nasser et al. successfully coated a nanostructured ANF interphase onto the surface of aramid fibers using a simple dip-coating process, resulting in a maximum increase of 25% in the short beam strength of aramid fiber reinforced composites [29]. However, ANFs are limited to considerably low concentrations inside these composites, whether through mixing them into the resin or adsorbing them to the surface, as agglomeration and dispersion problems reduce the mechanical performance. Moreover, the high thermal stability and low conductivity of ANFs prevent them from introducing multifunctionality to aramid composites.

Piezoelectric materials, such as zinc oxide nanowires (ZnO), have been shown to improve the interfacial properties of fiber reinforced composites while also introducing new functions, such as energy harvesting and damage detection [31–34]. Ehlert et al. reported a 55% increase in interfacial shear strength when zinc oxide nanowires were grafted onto the surface of aramid fibers [35]. Despite the hydrothermal synthesis process and the preservation of fiber strength, the need for multiple successive growth reactions to reach optimal nanowire aspect ratios limits the scalability of such a method. Another widely popular nanomaterial is carbon nanotubes (CNTs), whose excellent mechanical, thermal, and electrical properties make it an ideal candidate as a multifunctional reinforcement in fiber reinforced composites [36]. While carbon fibers can be whiskerized with CNTs using chemical vapor deposition (CVD), the high operating temperature of such a process is incompatible with polymer fibers [37]. In addition, CVD is an expensive process with high energy consumption which causes it to be cost-ineffective and hard to scale to industrial levels. Other CNT grafting techniques require conductive fibers, thus making them unsuitable for aramid fibers [38,39]. Efforts to reinforce the matrix through the dispersion of CNTs into the resin have also been found to be infective, as agglomeration and considerable increase in resin viscosity severely reduce the ability of the CNTs to act as reinforcements [40,41]. Recent work aims to improve the mechanical properties of aramid fiber reinforced composites, such as tensile strength, flexural strength, and impact toughness, using CVD synthesized CNT bucky paper interleaves [42]. However, the study fails to address the effect of the CNT interleaves on the interlaminar properties of the composite.

Alternatively, Lin et al. demonstrated the ability to generate 3D porous graphene on commercial polyimide sheets through a simple laser induction process [43]. The rapid and cost-effective process has been heavily exploited in a wide range of applications, such as soft electronics and memory devices [44,45]. The induction process was further developed to show the ability to control the laser induced graphene (LIG) morphology through the impulse density of the laser, allowing for the transformation of graphene sheets into graphene fibers [46]. Furthermore, Chyan et al. reported an expanded list of substrates on which the LIG could be directly generated which included a number of thermoplastics and thermosets, one of which is poly (paraphenylene terephthalamide), commercially known as Kevlar [47]. In this work, the mechanical performance of LIG coated aramid fiber reinforced composites is studied and their multifunctionality is demonstrated. Various morphologies of graphene are induced on Kevlar fabric using a laser induction process, and its effect on the mechanical performance of the composite is studied through short beam shear and Mode I fracture toughness testing. The tensile strength of the LIG coated fabric is also studied using tensile testing. The introduction of an LIG interlaminar region results in a substantial increase in both short beam shear strength and fracture toughness while preserving the specific strength of the aramid fabric. The improvement in mechanical properties is attributed to the enhanced chemical interaction and mechanical interlocking at the interlaminar region. The piezoresistive LIG is also shown to greatly increase the conductivity of both aramid fabric and aramid composites. The various LIG surface morphologies on the aramid fabric, along with post-testing fracture surfaces, are observed using scanning electron microscopy (SEM). Finally, further insight into the effect of the laser induction process on the aramid surface chemistry is studied through Raman and X-ray photoelectron spectroscopy (XPS) methods.

2. Experimental

2.1. Generation of LIG on aramid surface and chemical characterization

Kevlar® KM2+ unidirectional tape (style 790 scoured, CS-800) was cleaned through soaking in boiling acetone and ethanol before rinsing with deionized water and drying at 100 °C overnight under vacuum. The carbonization of the aramid fabric was achieved using the 60 W CO_2 laser of a universal laser system (Epilog Zing 24) operating in raster Mode (Fig. 1). Using the built-in software, the output power of the laser was varied between 8% and 20% in order to generate various surface morphologies, while the impulse per unit area and the laser raster speed were kept constant at 400 dots per inches (DPI) and 1 $cm^2 s^{-1}$, respectively. Two LIG configurations were fabricated, the first with LIG only on one side of the fabric, and a second where LIG was formed on both sides of the fabric, thus eliminating any interlaminar aramid region when infused with a resin matrix.

2.2. Surface characterization

The different aramid surface morphologies were imaged using a JEOL JSM-7800FLV field-emission scanning electron microscope. Changes to the chemical composition of the aramid fabric surface due to the laser induction process were characterized using XPS performed on a Kratos axis ultra XPS. Raman scattering of untreated and LIG coated aramid surfaces was also achieved using a Renishaw inVia confocal Raman microscope equipped with a 633 nm laser source.

2.3. Short beam shear testing

The multifunctional role of the LIG coated aramid fiber reinforced composites was evaluated using a series of mechanical testing. The short beam shear strength of the composites when coated with LIG at various laser output powers was measured according to ASTM D2344. The LIG coated aramid plies were infused with an EPON 862/curing agent W resin system (100:26.4) using vacuum-assisted resin transfer molding (VARTM). The infused fabric preforms were then pressed at 100 psi while curing at 177 °C for 3 h. Short beam specimens of 2.5 mm thickness were cut to dimensions of 15 mm by 5 mm, and 14 samples were tested for each data set at a constant span to thickness ratio of 4:1. When identical fabrication conditions were maintained, the LIG coated short beam specimens were found to have near identical thicknesses, relative to untreated composites (Fig. S1). The following eliminates thickness effects and allows for accurate comparison between the short beam performance of untreated and LIG coated composites [48]. The resistivity of the obtained specimens was measured using both a Keysight E4980AL LCR meter and the standard 4-point probe method. Silver paint was used to coat the perimeter of the specimens, before connecting it to 33-gauge magnet wires. Using a BK Precision® model 9130 triple output programmable DC power supply, a 4 mA DC current was applied to the specimen, and the voltage across of it was measured through a NI 4431 data acquisition system (DAQ).

2.4. Mode I testing

Mode I fracture toughness was obtained according to ASTM D5528-13. In this case, 16 plies of aramid fabric were used as preforms and a pre-crack length of 50 mm was achieved by inserting a Teflon sheet spacer midway through the thickness of the composite. The composite plates were fabricated using a similar VARTM process to the one mentioned above. Loading hinges were attached to either side of the 14 cm long, 23 mm wide, and 3 mm thick specimens using high shear strength epoxy (Loctite® 9430™ Hysol®) that was cured at 83 °C for 1 h. It should be noted that the mentioned pre-crack length does not include the space for the loading hinges of 11.2 mm. A minimum of six specimens per data set were loaded on an Instron universal load frame (Model 5982) at a crosshead speed of 2 mm/min until cracking was initiated. The samples were then unloaded back to their initial positions before reloading them at the same rate for the remainder of the test.

2.5. Fabric tensile testing

The effect of the laser induction process on the strength of the aramid fabric was quantified via fabric tensile testing. The tensile specimens consisted of rectangular strips containing 20 yarns with a gauge length of 75 mm. Proper gripping of the specimens was ensured by bonding three plies of the fabric to the ends of the samples using high shear strength epoxy (Loctite® 9430™ Hysol®) to act as tabs. The samples were all tested in the weft (fill) direction using the same universal load frame mentioned above and at a crosshead speed of 300 mm/min. Twelve specimens of each data set were loaded until failure to obtain the ultimate tensile strength and elongation of the fabric.

2.6. Damping properties measurement

Further characterization of the viscoelastic properties of the LIG coated aramid fiber reinforced composites was achieved using Dynamic Mechanical Thermal Analysis (DMTA) (Q800 analyzer from TA Instruments). The samples were loaded in a three-point

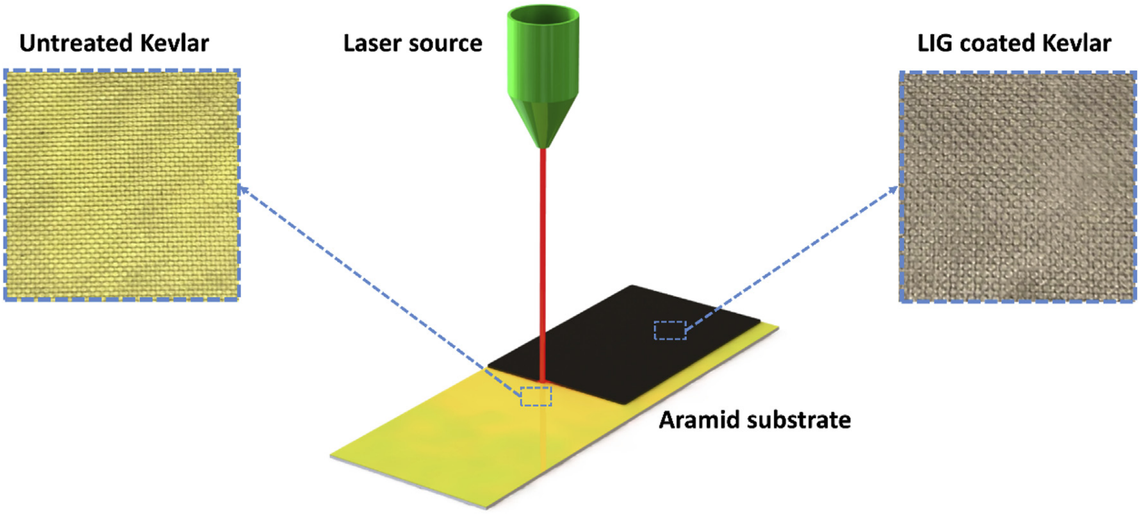

Fig. 1. Schematic of graphene laser induction process on aramid fabric. (A colour version of this figure can be viewed online.)

bending configuration using dual cantilever clamps at a frequency of 10 Hz. A heating rate of 5 °C/min was used, beginning at ambient temperature and increasing to 180 °C. The aramid composite beams were 60 mm in length, 10.5 mm in width, and ~1.1 mm in thickness. It should be noted that for all four mechanical tests, untreated aramid fiber reinforced composites and aramid fabric specimens were prepared and tested for comparison.

3. Results and discussion

3.1. Morphological and chemical characterization

The modified surface morphology due to the laser induction process is investigated using SEM imaging (Fig. 2, S2 & S3). Fig. 2a and b shows the aramid fabric surface consisting of smooth aramid fibers. Unlike carbon fibers, aramid fibers lack the striations and surface roughness required for a high degree of mechanical interlocking between the fiber and the matrix resin, which combined with the inert chemical structure, result in weak fiber-matrix interfaces. By subjecting the aramid substrate to laser induction, the surface morphology is considerably modified while being dependent on the output power of the process. Unlike the initially reported LIG fabrication method on polyimide films, the replication of this process on aramid substrates is achieved at considerably lower fluences than the reported critical value of 5.5 J cm^2 on polyimide substrates [46]. By defocusing the laser, the conversion of high temperature polymers, such as Kevlar, into amorphous carbon can be achieved at lower fluences, thus protecting the fiber from the ablation and considerable thermal damage which would otherwise diminish its performance [47]. In this case, the induction process was performed at a defocusing distance of 0.3 mm, raster speed of 1 cm^2, and impulse per unit area (IUA) of 400 DPI, while varying the induction power. The impulse density was chosen in order to generate forests of individual and distinct LIG micro-fibers instead of continuous micro-sheets [46]. As shown in Fig. 2c and d, at low output powers of 8 and 10%, the graphene induction process can be initiated but does not result in hierarchical surface morphology. At such low fluences, the induction process is limited to the top surface of the aramid fabric, limiting the formation of 3D microstructures that are capable of reinforcing the interlaminar region. Moreover, given the woven surface of aramid fabric, the resulting morphology was non-uniform as the amount of fluence varies at different locations on the substrate. Interestingly, at 12% output power, the aramid fibers were coated with a uniform sizing (Fig. 2e) and 3D structures appeared in the form of stiff, striated grooves and ridges (Fig. 2f and g). These morphological changes considerably increase the aramid fiber surface roughness and allow for a greater degree of interlocking between the fiber and matrix. In addition, the wettability of the fabric is also increased due to the fact that the aramid fabric is further embedded inside the matrix, thus significantly strengthening the interlaminar region. As the output power is increased to 16%, LIG forests begin to sporadically appear across the aramid substrate without any microstructure uniformity (Fig. 2h and i). Further increasing the output power to 20% results in a 3D LIG forest that uniformly coats the aramid fiber (Fig. 2j and k). The generated LIG micro-fibers possess aspect ratios ranging from 20 to 40, with lengths between 200 and 400 μm, and diameters between 10 and 15 μm. These LIG forests give the aramid fabric a surface morphology that is able to be firmly embedded and interlock with the matrix while also increasing interfacial interaction surface area, thus reinforcing the interlaminar region using a microstructure with great mechanical properties. Moreover, the porous nature of these micro-fibers, as seen in Fig. 2l, allows for facile resin wetting and infusion, eliminating the possibility of wicking and preserving the reinforcing capacity. It can thus be seen that the laser induction process on aramid substrates can result in LIG surface morphologies capable of multifunctional strengthening of the interlaminar region of aramid composites.

For further insight into the effect of the induction process on the aramid surface, the chemical composition of these surfaces was characterized. The graphitic nature of the laser induced aramid fabric was investigated using Raman spectroscopy (Fig. 3a and b). The Raman spectra of the untreated aramid fabric shows the characteristic peaks for PPTA, with the peaks at 1517 cm^{-1} and 1608.5 cm^{-1} corresponding to the C=C ring axial vibration mode, while those positioned at 1569 cm^{-1} and 1647 cm^{-1} belong to the

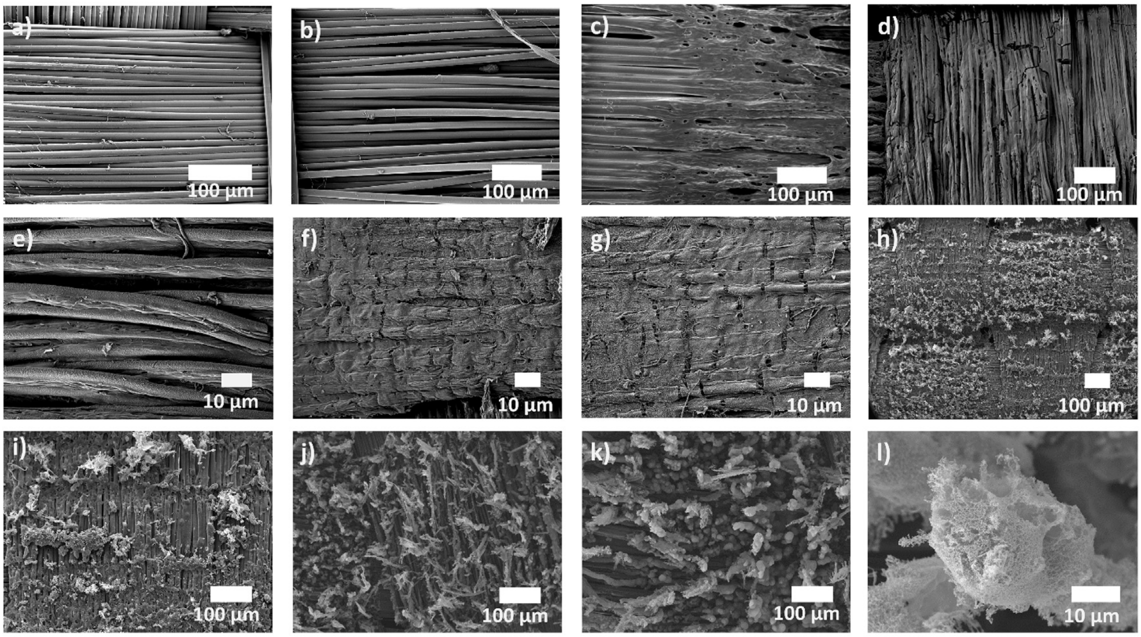

Fig. 2. Surface morphology of laser induced graphene on aramid fabric surface at various power outputs: a, b) 0%. c) 8%. d) 10%. e, f, g) 12%. h, i) 16%. j, k, l) 20%.

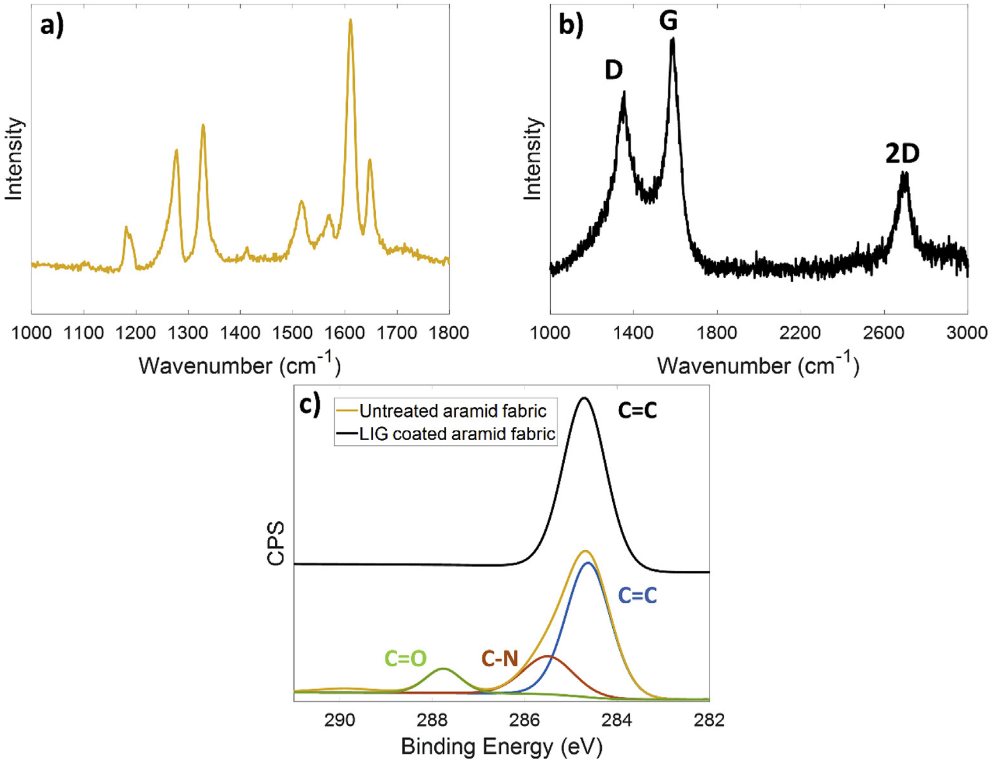

Fig. 3. Chemical characterization of untreated and LIG coated aramid fabric. a) Raman spectra of untreated aramid fabric. b) Raman spectra of LIG coated aramid fabric. c) XPS spectra of untreated and LIG coated aramid fabric. (A colour version of this figure can be viewed online.)

radial vibration mode originating at amide II and amide I, respectively. The high crystallinity of aramid fibers is primarily derived from the exact disposition of its monomers along both the axial and radial directions. Fig. 3b shows the Raman spectra of an LIG coated aramid fabric which displays the typical peaks of a graphitic structure D-band, G-band, and 2D-band at 1354 cm^{-1}, 1580 cm^{-1}, and 2699 cm^{-1}, respectively. As, expected, the degree of aramid fabric graphitization was found to increase with increasing power output of the induction (Fig. S4). The observed strong D peak is the result of defects and broken symmetry sites indicating a low LIG quality with an I_G/I_D ratio of 1.29. While the quality of the induced graphene on the aramid substrate is considerably lower than that observed on other substrates, such as polyimide and polyether ether ketone (PEEK), it is in agreement with other reported LIG-treated Kevlar fabric [47]. Nonetheless, the LIG remains capable of introducing multifunctionality to the aramid fabric in the form of a hierarchical micro-structured surface with high electrical conductivity, and can thus be further optimized depending on the application. The LIG coating is further characterized using XPS analysis of C1s spectrum, as seen in Fig. 3c. While the XPS spectra of the untreated aramid fabric can be deconvoluted into three bonding state peaks corresponding to C—C, C—N, and C═O at 284.7 eV, 285.9 eV, and 287.8 eV, respectively, the bonding state peak of the LIG coated aramid fabric is exclusively that of C—C. This indicate an increase in the aramid surface carbon content, as the content of other components, such as nitrogen and oxygen, is decreased due to graphitization.

3.2. Short beam and mode I fracture toughness testing

The merit of introducing LIG onto the aramid fibers reinforcing the composite can be assessed using various forms of mechanical testing. First, the effect of LIG on the interlaminar shear of the aramid composites was quantified using short beam shear (SBS) testing. Along with matrix toughness, interfacial adhesion is a critical factor in the SBS failure modes, therefore allowing for such testing to reveal any reinforcement to the interlaminar region due to the LIG. The SBS specimens were fabricated as described in ASTM D2344, in two distinct configurations, both shown in Fig. 4a. In the one-sided configuration, the LIG was generated solely on one side of the aramid fabric, resulting in inter-ply regions of thickness t with LIG-aramid interfaces. Using the double-sided configuration (D), an intermediate LIG-LIG interface was added inside the interlaminar region, due to the LIG coating on both sides of the aramid fabric. In this case, three interfacial regions are created, with two of them being LIG-aramid interfacial regions and the third region containing the graphitic interface at the intersection of both LIG layers. The interlaminar behavior of the fabricated composites is dependent on the chemical interaction and mechanical interlocking between the fabric and the matrix due to these interfacial reinforcements. The presence of the LIG inside aramid composites is confirmed using an optical microscope (Fig. 4b and c), which shows uniform and continuous LIG coated interlaminar regions. This is further characterized using SEM imaging, which shows thin interlaminar regions of less than 15 μm for aramid composites reinforced with LIG in the double-sided configuration (Fig. 4d and e). The thin nature of the interlayer reinforcement is important to preserve the desired composite properties by reducing the number of polymer-rich regions that are devoid from any in-plane reinforcement. As seen in Fig. 4f, the SBS strength of LIG coated aramid fiber reinforced composites was found to be increased independent of induction power and LIG configuration (one-sided or double-sided), relative to that of untreated aramid composites. A maximum improvement of 70% in SBS strength was observed at an induction power of 12% in the one-sided configuration relative to the untreated fabric, whereas LIG induced at 20% in the one-sided

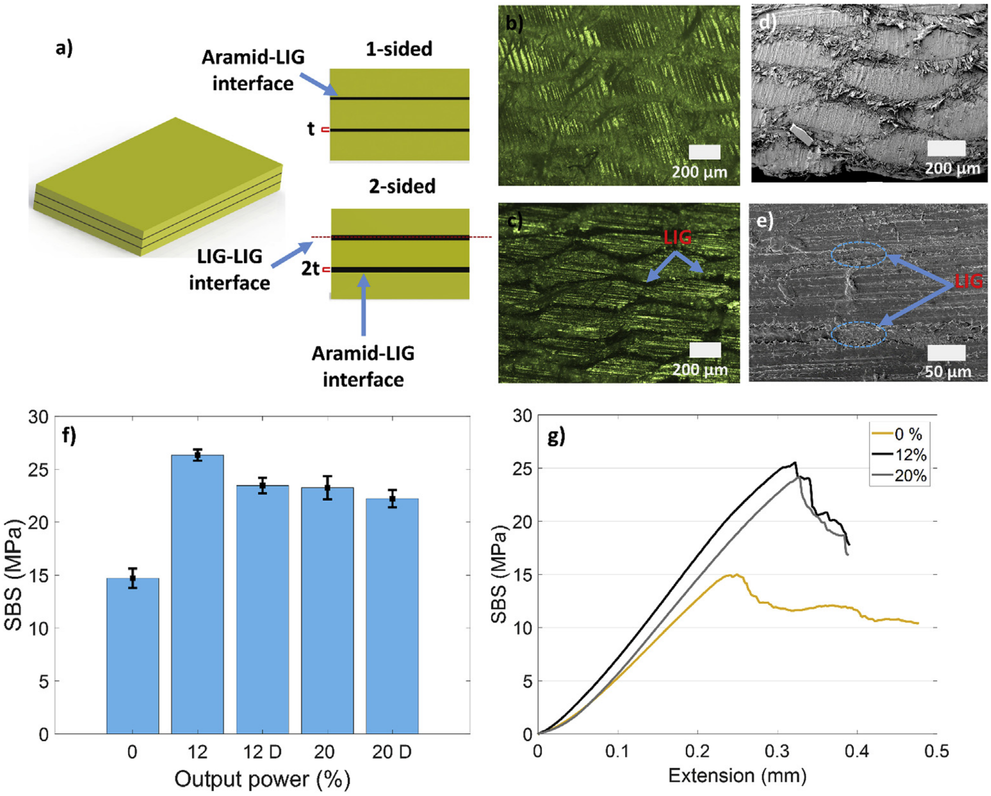

Fig. 4. a) Short beam aramid fiber reinforced composite specimens in both the one-sided and double-sided configuration. Each LIG layer is of thickness t. b) Optical microscope image of the cross-section of untreated aramid fiber reinforced composites. c) Optical microscope image of the cross-section of LIG coated aramid fiber reinforced composites. d, e) SEM images of the interlaminar region inside LIG coated aramid fiber reinforced composites. f) Short beam strength of LIG coated aramid fiber reinforced composites at various induction power and configurations. g) Corresponding stress-extension curves of loaded short beam specimens. (A colour version of this figure can be viewed online.)

configuration resulted in only 55% improvement. This indicates that the morphology of the grooves and ridges at 12% lead to a slightly higher degree of interlaminar reinforcement than the LIG microfibers at 20%. This can be attributed to the stiffer nature of the former in comparison to the fuzzy structure of the latter. Nonetheless, both sets of LIG microstructures enhance the resistance of the composites to shear stress and allow for a higher ability to withstand induced deformation. The observed improvement is derived from an enhanced adhesion between the fiber and the resin as the LIG becomes anchored inside the epoxy matrix. The LIG results in hierarchical composites where interlaminar discontinuities are bridged, thus allowing for improved transfer of loads between the fiber and matrix, therefore limiting interlaminar failure. Moreover, graphene has been shown to improve mechanical properties, such as fracture toughness and flexural modulus, of epoxy polymer matrices when in the form of nanocomposites [49–52]. By toughening the matrix, the LIG further reinforces the interlaminar region and results in higher shear strength. Although the double-sided configuration at both induction powers resulted in up to 53% increase in SBS strength relative to untreated aramid composites, its performance was found to be 11.3% and 8.8% inferior to that of the one-sided configuration at 12% and 20%, respectively. This slight decrease in reinforcement capability can be explained by the possible weak interlocking at the LIG-LIG interface, causing a slightly more discontinuous and defective interlaminar region relative to that obtained in the one-sided configuration. It should be noted that along with its mechanical advantages, LIG has been shown to possess excellent electrical properties, particularly piezoresistivity, allowing for the introduction of conductivity into the traditionally insulating aramid fiber reinforced composites. The resistivity across the top of the LIG coated SBS specimens at 12% induction power and in the one-sided configuration was found to range between and 0.291 Ω m and 0.449 Ω m, while that of the double-sided configuration varied between 0.162 Ω m and 0.291 Ω m. Once induction power is increased to 20%, the resistivity of the specimens considerably drops to range between and 0.0331 Ω m and 0.0645 Ω m for the one-sided configuration, and between 0.0155 Ω m and 0.031 Ω m for the double sided one. Moreover, the double-sided configuration was also found to be conductive through the thickness of the sample. This unlocks great potential for the embedding of numerous unprecedented functions into aramid composites such as strain sensing, damage detection, joule heating, and controlling surface wetting properties [45]. The introduced multifunctionality will help reduce the weight and complexity of aramid fiber reinforced composites by eliminating the need for certain external sensors and actuators.

Further understanding of the reinforcement mechanism due to the LIG coating is gained through inspection of the stress-displacement curves during SBS testing. The excellent fracture toughness of aramid fiber reinforced composites is a result of their inelastic deformation failure mode under shear loading [53]. As shown in Fig. 4g, untreated aramid SBS specimens do not exhibit a significant drop in stress at failure and are able to maintain steady stress loading until the completion of the test thus demonstrating high toughness. However, the observed response is changed in the presence of LIG, as the treated SBS specimens display a considerable increase in peak stress, relative to the untreated specimens, which is followed by a discontinuous decrease until reaching a final residual stress. Such loading behavior incorporates features of interlaminar shear into the predominant inelastic deformation aramid failure mode. A more common failure mode of carbon and glass fiber reinforced composites, interlaminar shear is characterized by high SBS strength along with large and sharp drops in stress post-failure, insinuating a more brittle behavior [54]. Nonetheless, the SBS failure mode of the LIG coated composites remains dominated by inelastic deformation, as the specimens do not display any visible delamination or cracking along the mid-plane. Furthermore, the LIG coating results in an increase in SBS stiffness due to a combination of the addition of graphitic interlayers and toughening of the epoxy matrix. This observation is consistent with reported studies in the literature that use carbon-based reinforcement, such as CNTs [55,56]. Therefore, LIG coated aramid fiber composites exhibit higher short beam strength and stiffness, while maintaining their unique toughness that is derived from their conserved inelastic deformation failure mode.

In practice, composites are often subjected to more complex loading conditions which combine various forms of stresses such as axial, compressive, and shear. Therefore, a reinforcement of the interlaminar region of aramid fiber reinforced composites is expected to be reflected through an improvement of its mechanical response to combinations of these stresses. A critical property of aramid fiber reinforced composites is their ability to delay damage initiation and propagation when under structural loading. A method to quantify and assess this characteristic is Mode I interlaminar fracture toughness testing, where double cantilever beam specimens are simultaneously subjected to tensile and shear loading (Fig. 5). The resistance of the composite to slow and stable propagation of initiated mid-plane cracking is measured in terms of fracture toughness obtained through modified beam theory (MBT). It should be noted that the interlaminar region in Mode I specimens was found to be larger than that in SBS specimens due to the effect of the Teflon insert used for pre-crack initiation (Fig. 5a). As seen in Fig. 5c, a maximum increase in fracture toughness of 540 J/m^2 was observed in samples coated with LIG at 20% induction power and in the one-sided configuration, resulting in a 20% improvement when compared to untreated aramid composites (462 J/m^2). The statistical significance of the improvement is further confirmed using one-way ANOVA analysis at a p-value of <0.01. The increase in fracture toughness of LIG coated aramid composites is the result of the enhanced interfacial bonding between the aramid fibers and the matrix. However, unlike short beam testing, the LIG induced micro-fiber morphology generated at 20% output power shows better Mode I fracture resistance than LIG induced at 12%. This is attributed to the 3D micro-structure of the LIG micro-fibers, which effectively bridges between adjacent plies during crack propagation, potentially acting as “nanostitches” [56–59]. Other carbon-based nanostructures of similar morphology, such as CNTs, have been shown to suppress delamination in fiber reinforced composites using comparable mechanisms. The difference in the optimal LIG morphology inside aramid fiber reinforced composites for SBS and Mode I testing can be attributed to the difference in failure modes between the two tests. During short beam testing, the LIG coated specimens fail primarily due to inelastic deformation without any signs of delamination. Such failure mode favors the rougher LIG morphology generated at 12%, as its superior mechanical interlocking performance allows for a higher resistance to shear stresses. However, during Mode I testing, the propagating crack causes clear delamination inside the composite. Under such conditions, the LIG micro-fibers generated at 20% can hinder the initiation and propagation of the crack, necessitating a larger fracture energy to achieve delamination. Visual inspection of the fracture surface of double cantilever beams show that only those containing a 20% LIG in the one-sided configuration present LIG residues on both surfaces, despite being introduced on only one of the plies (Fig. S6). This confirms that the following LIG morphology is capable of suppressing the propagation of cracks and delamination through a bridging mechanism, that can be only exploited during Mode I testing. A more suitable technique to determine the performance of the LIG under loading conditions that mimics that of SBS would be Mode II fracture toughness using end notch flexure specimens. However, the following test is not applicable to aramid composites, as their ability to absorb large mid-span deformations causes an unstable propagation of cracks. Similar to the SBS testing results, the double-sided configuration results in weaker fracture toughness relative to the one-sided configuration at a similar induction power. This observation confirms that the LIG-LIG interface presented in the double-sided configuration reduces the effectiveness of the reinforcement due to weakening of the mechanical reinforcement and the formation of agglomerations inside the matrix.

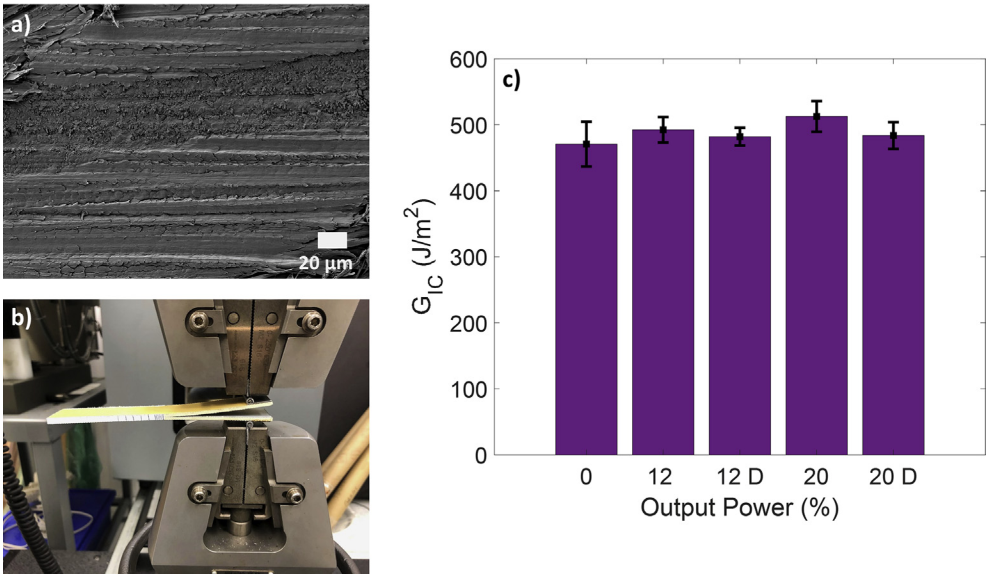

Fig. 5. a) SEM image of the interlaminar region inside Mode I LIG coated aramid fiber reinforced composite sample. b) Mode I experimental setup. c) Mode I fracture toughness of LIG composites at various induction power and configurations. (A colour version of this figure can be viewed online.)

Greater understanding of the reinforcement mechanism due to the addition of LIG within aramid composites can be obtained through post-testing micrographs of the delaminated surfaces of double cantilever Mode I specimens. Due to the weak interfacial bonding and interlaminar strength of untreated aramid composites, delamination occurs in an easy and clean manner as displayed by the smooth aramid fiber surfaces in Fig. 6a & S5. Given the weak adhesion between the untreated aramid fiber and the matrix, interfacial debonding is the primary cause of failure in untreated Mode I specimens. In contrast, LIG coated specimens show a considerable amount of epoxy resin residue remaining in the form of plates on the fractured aramid surface (Fig. 6b and c). Moreover, the fractured aramid surface is found to be considerably coarser than that of untreated fibers, as a layer of resin remains adhered to the surface (Fig. 6d). By transitioning interlaminar failure from an adhesive mode to a cohesive one, the fiber-matrix interface of the aramid fiber reinforced composites can withstand higher loads as cracks propagate inside the resin bulk. This is further supported by the revealed LIG on the fractured surfaces seen in Fig. 6e and f, which suggests strong adhesion between the resin and the LIG. The following is also supported by simple visual inspection of the fracture surfaces (Fig. S6). Moreover, the limited increase in fracture toughness is possibly due to the inability of current fracture toughness testing methods to account for reinforcing effects which prohibit or reduce intralaminar failure. However, such a claim requires further verification and investigation using techniques such as micro-computed tomography (CT) scan imagery. Thus, the following failure behavior shows the ability of the LIG to reinforce the aramid fiber-matrix interface, thus resulting in stronger interlaminar regions that fail in a cohesive manner under Mode I loading.

3.3. Tensile and damping properties

While LIG allows for the improvement of out-of-plane properties, it remains critical that the interlaminar reinforcement does not reduce the in-plane properties of the composite. The tensile strength of composites depends primarily on the quality and properties of the fiber or fabric provides in-plane reinforcement inside composites. Many techniques for growing nanomaterials onto fiber surfaces have been shown to result in etching and defect formation, thus failing to maintain the tensile properties of the fiber [37,60]. This is caused by the harsh synthesis conditions, such as high temperatures or the use of catalysts, thus leading to research focusing on the development of more benign grafting techniques, namely hydrothermal reactions [35,61,62]. In comparison, the LIG in this work is synthesized using a photo-thermal conversion process by means of pulsed laser irradiation, and its effect on aramid fabrics was investigated using fabric tensile testing. When compared to the tensile strength of untreated aramid fabric (3.22 GPa), the tensile strength of LIG coated aramid fabric is observed to decrease with increasing induction power, yielding up to 16.4% decrease in strength at 20% output power in the double side configuration (2.71 GPa) (Fig. 7a). Moreover, at constant induction powers of 12% and 20%, the double-sided configuration is additionally weakened relative to fabric coated only on one side, showing 2% and 7% further decrease in tensile strength, respectively. By generating LIG on the aramid surface, in-plane reinforcement is reduced at the expense of out-of-plane reinforcement, as aramid fibers are irradiated into graphitic microstructure with normal orientation relative to the substrate. Post-laser induction, the amount of aramid fibers inside the fabric along both the weft and warp directions is decreased, thus reducing its ability to support tensile and compressive loads. This is undesirable for composite applications, as it yields aramid fiber reinforced composites with weaker structural and ballistic performance. However, the induction process also results in a decrease in the weight of the aramid fabric; Fig. 7b shows maximum reduction in the areal density of the fabric of up to 17% when induction power reaches 20%. Similarly, the double-sided configuration further lowers the areal density, relative to the one-sided configuration, independent of induction power. These changes to the areal density were obtained by measuring the weight of a constant aramid fabric area before and after the induction of the LIG. Given that the induction process has been quantified through weight yields in previous studies, a weight approach was chosen over a volumetric one to describe the changes to the composition of the fabric [43,47]. The considerably low yield of the laser induction process insinuate that the measured weight is primarily that of the aramid fabric. Moreover, the decrease in weight with increasing output power is an expected outcome, as a thicker layer of aramid is transformed into LIG when exposed to a stronger irradiation process. This confirms that the decrease in tensile properties is not due to diminishing individual fiber strength during the treatment, but rather to the conversion of PPTA into LIG and gaseous products, as the induction process uses the surface of aramid fibers as reactants, thus

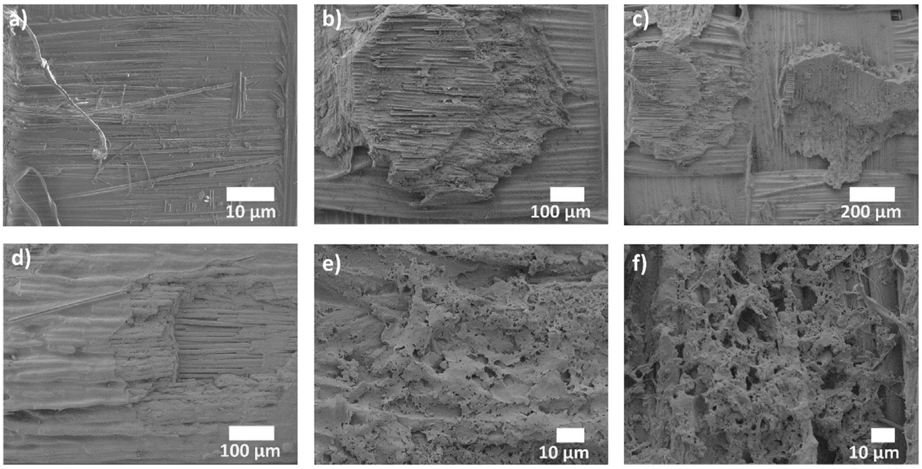

Fig. 6. Fracture surfaces of untreated and LIG coated aramid fiber reinforced composites following Mode I testing. a) Untreated aramid fiber reinforced composite. b, c, d, e, f) 20% LIG coated aramid fiber reinforced composite.

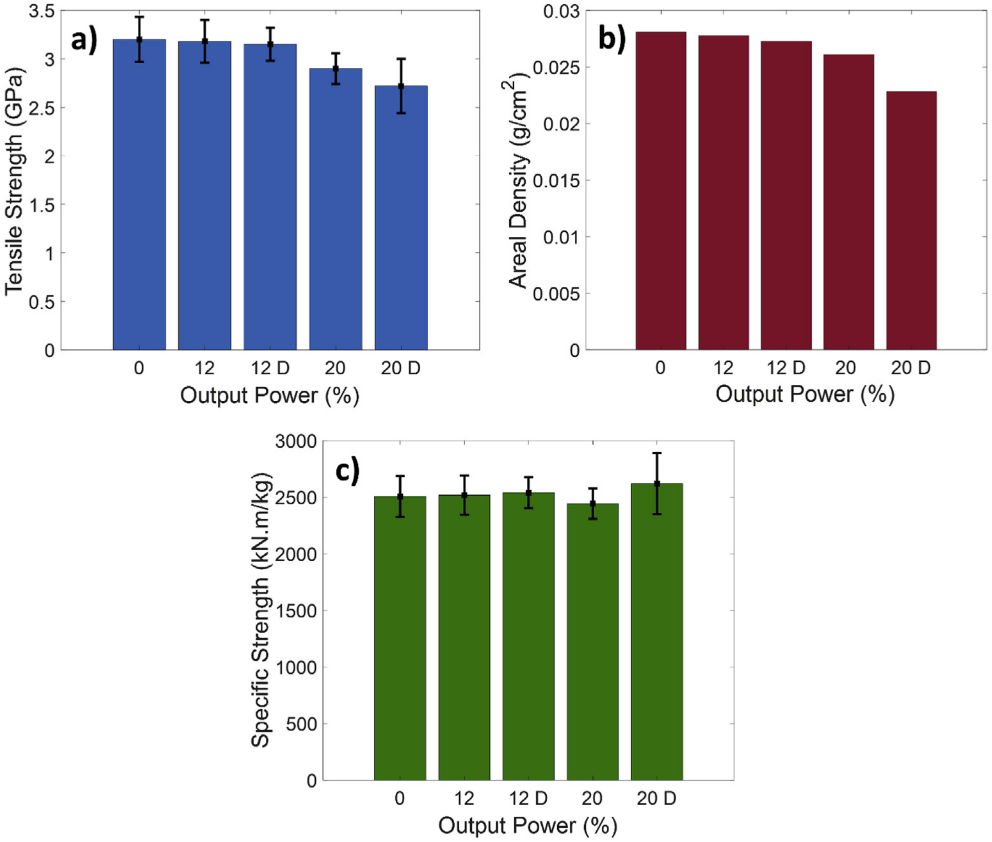

Fig. 7. a) Tensile strength of bare and LIG coated aramid fabric at various induction power and configurations. b) Areal density of bare and LIG coated aramid fabric at various induction power and configurations. c) Specific strength of bare and LIG coated aramid fabric at various induction power and configurations. (A colour version of this figure can be viewed online.)

decreasing the overall weight of the fabric. Therefore, as seen in Fig. 7c, none of the LIG coated fabrics display any statistical decrease in specific strength when compared to bare fibers, leading to the conclusion that the LIG coating results in out of plane reinforcement while maintaining the original specific strength of the fibers. It is then possible to fabricate lightweight LIG coated aramid fiber reinforced composite structures with preserved in-plane properties and an improved out-of-plane performance.

In addition to the preservation of in-plane properties, the introduction of the LIG does not interfere with the viscoelastic and damping behavior of the aramid fiber reinforced composite. Aramid composites are highly used in dynamic loading applications, such as in hard body armor and blast protection, due to their excellent energy absorption abilities [63]. Therefore, improvements to the structural performance are ideally desired while maintaining good dynamic response. Although viscoelastic properties are heavily dominated by the matrix, modification to the interlaminar and interfacial regions can alter the dynamic response of the composite [64,65]. The effect of these interlaminar modifications were studied through dynamic mechanical thermal analysis (DMTA) performed in the three-point bending configuration. The specific storage modulus (E′) and loss modulus (E″) were obtained through a normalization similar to the one reported in the previous section. This allows for more accurate assessment of the influence of the LIG on the response of the composite by accounting for the decrease in weight of the in-plane reinforcement. Fig. 8 shows unchanged specific viscoelastic properties when LIG aramid composite specimens are compared to untreated ones. The unaffected specific storage and loss modulus insinuates a preservation of the flexural rigidity and energy dissipation performance of the composite, respectively (Fig. 8a and b). Given that the loss tangent is the ratio of E″ to E’, the damping behavior of the aramid composite is expected to be conserved as seen in Fig. 8c. This indicates that the damping properties of the aramid fiber reinforced composites are preserved, while maintaining the same elastic and viscous response. It should be noted that similar trends were found irrespective of the LIG morphology, induction power, or configuration, thus only the case of laser induction at 20% and in the double-sided configuration is reported due to it having the most effect on the weight of the fabric and thus potentially its dynamic response. Finally, the LIG coated aramid specimens display an increase of 3.4 °C in the glass transition temperature (T_g), relative to that of untreated specimens, therefore allowing for slightly higher operating temperatures of the aramid composites.

4. Conclusions

This study has demonstrated the improvement of the mechanical properties and induced multifunctionality of aramid fiber reinforced composites through LIG coatings on aramid fabric. The laser induction process results in uniform graphene microstructures whose morphology can be controlled using induction power and pulsing density. The LIG based hierarchical aramid composites display improvement in mechanical performance due to an increase in mechanical interlocking and chemical interaction between the fabric and the matrix. The modified interlaminar region leads to a 70% improvement in short beam strength and 20% increase in Mode I fracture toughness of aramid fiber reinforced composites using an LIG generated at 12% and 20%, respectively. The chemical composition of the treated aramid fabric surface is

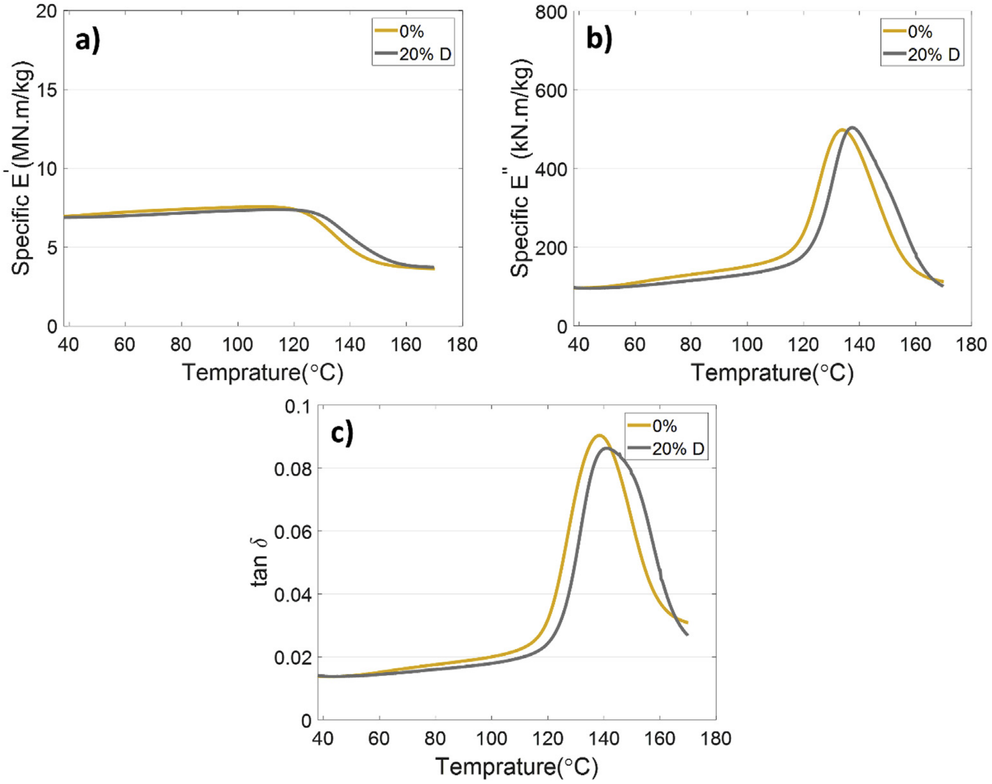

Fig. 8. Dynamic mechanical thermal analysis of untreated and LIG coated aramid fiber reinforced composites. a) Specific storage modulus. b) Specific loss modulus. c) Loss tangent. (A colour version of this figure can be viewed online.)

found to be consistent with that of graphene, while it's specific strength and damping properties is fully preserved post-treatment. In addition, the piezoresistive properties of the LIG allows for the expansion of the functionality of aramid composites. The method presented in this work allows for the design of aramid fiber-epoxy matrix interlaminar regions in a fast, simple, and cost-effective manner, therefore allowing it to be scaled up to industrial levels for the production of high strength and multifunctional aramid fiber reinforced composites.

Declaration of competing interest

The authors declare that they have no known competing financial interests or personal relationships that could have appeared to influence the work reported in this paper.

Acknowledgments

The authors gratefully acknowledge financial support for this research from the Army Research Office (Contract #W911NF-18-1-0061).

Appendix A. Supplementary data

Supplementary data to this article can be found online at https://doi.org/10.1016/j.carbon.2019.11.078.

References

[1] V.P. McConnell, Ballistic protection materials a moving target, Reinforc Plast 50 (2006) 20–25, https://doi.org/10.1016/S0034-3617(06)71187-0.
[2] T.J. Singh, S. Samanta, Characterization of kevlar fiber and its composites: a review, Mater. Today Proc. 2 (2015) 1381–1387, https://doi.org/10.1016/J.MATPR.2015.07.057.
[3] J.-K. Kim, Y.W. Mai, Engineered Interfaces in Fiber Reinforced Composites, Elsevier Sciences, 1998.
[4] R.F. Gibson, Principles of Composite Material Mechanics, fourth ed., CRC Press, 2016.
[5] X. Wang, X. Fu, D.D.L. Chung, Strain sensing using carbon fiber, J. Mater. Res. 14 (1999) 790–802, https://doi.org/10.1557/JMR.1999.0105.
[6] S.A. Hayes, A.D. Lafferty, G. Altinkurt, P.R. Wilson, M. Collinson, P. Duchene, Direct Electrical Cure of Carbon Fiber Composites, 2015, https://doi.org/10.1179/2055035915Y.0000000001.
[7] G. Kister, B. Ralph, G.F. Fernando, Damage detection in glass fibre-reinforced plastic composites using self-sensing E-glass fibres, Smart Mater. Struct. 13 (2004) 1166–1175, https://doi.org/10.1088/0964-1726/13/5/021.
[8] J. Wen, Z. Xia, F. Choy, Damage detection of carbon fiber reinforced polymer composites via electrical resistance measurement, Compos. Part B. 42 (2011) 77–86, https://doi.org/10.1016/j.compositesb.2010.08.005.
[9] J. Han, H. Zhang, M. Chen, D. Wang, Q. Liu, Q. Wu, Z. Zhang, The combination of carbon nanotube buckypaper and insulating adhesive for lightning strike protection of the carbon fiber/epoxy laminates, Carbon N. Y. 94 (2015) 101–113, https://doi.org/10.1016/J.CARBON.2015.06.026.
[10] P. Lee-Sullivan, K.S. Chian, C.Y. Yue, H.C. Looi, Effects of bromination and hydrolysis treatments on the morphology and tensile properties of Kevlar-29 fibres, J. Mater. Sci. Lett. 13 (1994) 305–309, https://doi.org/10.1007/BF00420781.
[11] B. Gao, R. Zhang, F. Gao, M. He, C. Wang, L. Liu, L. Zhao, H. Cui, Interfacial microstructure and enhanced mechanical properties of carbon fiber composites caused by growing generation 1–4 dendritic poly(amidoamine) on a fiber surface, Langmuir 32 (2016) 8339–8349, https://doi.org/10.1021/acs.langmuir.6b01485.
[12] G.S. Sheu, S.S. Shyu, Surface properties and interfacial adhesion studies of aramid fibres modified by gas plasmas, Compos. Sci. Technol. 52 (1994) 489–497, https://doi.org/10.1016/0266-3538(94)90031-0.
[13] S.R. Wu, G.S. Sheu, S.S. Shyu, Kevlar fiber-epoxy adhesion and its effect on composite mechanical and fracture properties by plasma and chemical treatment, J. Appl. Polym. Sci. 62 (1996) 1347–1360, https://doi.org/10.1002/(SICI)1097-4628(19961128)62:9<1347::AID-APP5>3.0.CO;2-H.
[14] G.J. Ehlert, Y. Lin, H.A. Sodano, Carboxyl functionalization of carbon fibers through a grafting reaction that preserves fiber tensile strength, Carbon N. Y. 49 (2011) 4246–4255, https://doi.org/10.1016/j.carbon.2011.05.057.
[15] J. Wang, P. Chen, X. Xiong, C. Jia, Q. Yu, K. Ma, Interface characteristic of aramid fiber reinforced poly(phthalazinone ether sulfone ketone) composite, Surf. Interface Anal. 49 (2017) 788–793, https://doi.org/10.1002/sia.6224.
[16] G.J. Ehlert, Y. Lin, H.A. Sodano, Carboxyl functionalization of carbon fibers through a grafting reaction that preserves fiber tensile strength, Carbon N. Y. 49 (2011) 4246–4255, https://doi.org/10.1016/J.CARBON.2011.05.057.
[17] J. Nasser, J. Lin, H. Sodano, High strength fiber reinforced composites with

surface fibrilized aramid fibers, J. Appl. Phys. 124 (2018), 045305, https://doi.org/10.1063/1.5026987.

[18] L. Liu, Y.D. Huang, Z.Q. Zhang, Z.X. Jiang, L.N. Wu, Ultrasonic treatment of aramid fiber surface and its effect on the interface of aramid/epoxy composites, Appl. Surf. Sci. 254 (2008) 2594–2599, https://doi.org/10.1016/J.APSUSC.2007.09.091.

[19] H. Dong, J. Wu, G. Wang, Z. Chen, G. Zhang, The ultrasound-based interfacial treatment of aramid fiber/epoxy composites, J. Appl. Polym. Sci. 113 (2009) 1816–1821, https://doi.org/10.1002/app.30055.

[20] R. Benrashid, G.C. Tesoro, Effect of surface-limited reactions on the properties of Kevlar® fibers, Text. Res. J. 60 (1990) 334–344, https://doi.org/10.1177/004051759006000604.

[21] R. Sa, Y. Yan, Z. Wei, L. Zhang, W. Wang, M. Tian, Surface modification of aramid fibers by Bio-inspired poly(dopamine) and epoxy functionalized silane grafting, ACS Appl. Mater. Interfaces 6 (2014) 21730–21738, https://doi.org/10.1021/am507087p.

[22] B.A. Patterson, H.A. Sodano, Enhanced interfacial strength and UV shielding of aramid fiber composites through ZnO nanoparticle sizing, ACS Appl. Mater. Interfaces 8 (2016) 33963–33971, https://doi.org/10.1021/acsami.6b07555.

[23] B. Wang, Y. Duan, J. Zhang, Titanium dioxide nanoparticles-coated aramid fiber showing enhanced interfacial strength and UV resistance properties, Mater. Des. 103 (2016) 330–338, https://doi.org/10.1016/j.matdes.2016.04.085.

[24] J. Juntaro, M. Pommet, A. Mantalaris, M. Shaffer, A. Bismarck, Nanocellulose enhanced interfaces in truly green unidirectional fibre reinforced composites, Compos. Interfac. 14 (2007) 753–762, https://doi.org/10.1163/156855407782106573.

[25] K.-Y. Lee, Y. Aitomäki, L.A. Berglund, K. Oksman, A. Bismarck, On the use of nanocellulose as reinforcement in polymer matrix composites, Compos. Sci. Technol. 105 (2014) 15–27, https://doi.org/10.1016/j.compscitech.2014.08.032.

[26] J. Jang, J. Bae, K. Lee, Synthesis and characterization of polyaniline nanorods as curing agent and nanofiller for epoxy matrix composite, Polymer 46 (2005) 3677–3684, https://doi.org/10.1016/j.polymer.2005.03.030.

[27] J. Lin, S.H. Bang, M.H. Malakooti, H.A. Sodano, Isolation of aramid nanofibers for high strength and toughness polymer nanocomposites, ACS Appl. Mater. Interfaces 9 (2017) 11167–11175, https://doi.org/10.1021/acsami.7b01488.

[28] B.A. Patterson, M.H. Malakooti, J. Lin, A. Okorom, H.A. Sodano, Aramid nanofibers for multiscale fiber reinforcement of polymer composites, Compos. Sci. Technol. 161 (2018) 92–99, https://doi.org/10.1016/j.compscitech.2018.04.005.

[29] J. Nasser, J. Lin, K. Steinke, H.A. Sodano, Enhanced interfacial strength of aramid fiber reinforced composites through adsorbed aramid nanofiber coatings, Compos. Sci. Technol. 174 (2019) 125–133, https://doi.org/10.1016/J.COMPSCITECH.2019.02.025.

[30] M. Yang, K. Cao, L. Sui, Y. Qi, J. Zhu, A. Waas, E.M. Arruda, J. Kieffer, M.D. Thouless, N.A. Kotov, Dispersions of aramid nanofibers: a new nanoscale building block, ACS Nano 5 (2011) 6945–6954, https://doi.org/10.1021/nn2014003.

[31] Y. Lin, G. Ehlert, H.A. Sodano, Increased interface strength in carbon fiber composites through a ZnO nanowire interphase, Adv. Funct. Mater. 19 (2009) 2654–2660, https://doi.org/10.1002/adfm.200900011.

[32] U. Galan, Y. Lin, G.J. Ehlert, H.A. Sodano, Effect of ZnO nanowire morphology on the interfacial strength of nanowire coated carbon fibers, Compos. Sci. Technol. 71 (2011) 946–954, https://doi.org/10.1016/j.compscitech.2011.02.010.

[33] M.H. Malakooti, B.A. Patterson, H.-S. Hwang, H.A. Sodano, ZnO nanowire interfaces for high strength multifunctional composites with embedded energy harvesting, Energy Environ. Sci. 9 (2016) 634–643, https://doi.org/10.1039/C5EE03181H.

[34] L. Groo, D.J. Inman, H.A. Sodano, In situ damage detection for fiber-reinforced composites using integrated zinc oxide nanowires, Adv. Funct. Mater. 28 (2018), 1802846, https://doi.org/10.1002/adfm.201802846.

[35] G.J. Ehlert, H.A. Sodano, Zinc oxide nanowire interphase for enhanced interfacial strength in lightweight polymer fiber composites, ACS Appl. Mater. Interfaces 1 (2009) 1827–1833, https://doi.org/10.1021/am900376t.

[36] E.T. Thostenson, Z. Ren, T.-W. Chou, Advances in the science and technology of carbon nanotubes and their composites: a review, Compos. Sci. Technol. 61 (2001) 1899–1912, https://doi.org/10.1016/S0266-3538(01)00094-X.

[37] Q. Zhang, J. Liu, R. Sager, L. Dai, J. Baur, Hierarchical composites of carbon nanotubes on carbon fiber: influence of growth condition on fiber tensile properties, Compos. Sci. Technol. 69 (2009) 594–601, https://doi.org/10.1016/J.COMPSCITECH.2008.12.002.

[38] Q. An, A.N. Rider, E.T. Thostenson, Electrophoretic deposition of carbon nanotubes onto carbon-fiber fabric for production of carbon/epoxy composites with improved mechanical properties, Carbon N. Y. 50 (2012) 4130–4143, https://doi.org/10.1016/J.CARBON.2012.04.061.

[39] E. Bekyarova, E.T. Thostenson, A. Yu, H. Kim, J. Gao, J. Tang, H.T. Hahn, T.-W. Chou, M.E. Itkis, R.C. Haddon, Multiscale carbon Nanotube–Carbon fiber reinforcement for advanced epoxy composites, Langmuir 23 (2007) 3970–3974, https://doi.org/10.1021/LA062743P.

[40] M. Tehrani, A.Y. Boroujeni, T.B. Hartman, T.P. Haugh, S.W. Case, M.S. Al-Haik, Mechanical characterization and impact damage assessment of a woven carbon fiber reinforced carbon nanotube–epoxy composite, Compos. Sci. Technol. 75 (2013) 42–48, https://doi.org/10.1016/J.COMPSCITECH.2012.12.005.

[41] F.H. Gojny, M.H.G. Wichmann, U. Köpke, B. Fiedler, K. Schulte, Carbon nanotube-reinforced epoxy-composites: enhanced stiffness and fracture toughness at low nanotube content, Compos. Sci. Technol. 64 (2004) 2363–2371, https://doi.org/10.1016/j.compscitech.2004.04.002.

[42] S. Sharma, S.R. Dhakate, A. Majumdar, B.P. Singh, Improved static and dynamic mechanical properties of multiscale bucky paper interleaved Kevlar fiber composites, Carbon N. Y. (2019), https://doi.org/10.1016/J.CARBON.2019.06.055.

[43] J. Lin, Z. Peng, Y. Liu, F. Ruiz-Zepeda, R. Ye, E.L.G. Samuel, M.J. Yacaman, B.I. Yakobson, J.M. Tour, Laser-induced porous graphene films from commercial polymers, Nat. Commun. 5 (2014), 5714, https://doi.org/10.1038/ncomms6714.

[44] R. Ye, D.K. James, J.M. Tour, Laser-induced graphene: from discovery to Translation, Adv. Mater. 31 (2019), 1803621, https://doi.org/10.1002/adma.201803621.

[45] D.X. Luong, K. Yang, J. Yoon, S.P. Singh, T. Wang, C.J. Arnusch, J.M. Tour, Laser-induced graphene composites as multifunctional surfaces, ACS Nano (2019), https://doi.org/10.1021/acsnano.8b09626 acsnano.8b09626.

[46] L.X. Duy, Z. Peng, Y. Li, J. Zhang, Y. Ji, J.M. Tour, Laser-induced graphene fibers, Carbon N. Y. 126 (2018) 472–479, https://doi.org/10.1016/J.CARBON.2017.10.036.

[47] Y. Chyan, R. Ye, Y. Li, S. Pratap Singh, C.J. Arnusch, J.M. Tour, Laser-induced graphene by multiple lasing: toward electronics on cloth, paper, and food article, ACS Nano 12 (2018), https://doi.org/10.1021/acsnano.7b08539.

[48] W. Cui, M.R. Wisnom, M. Jones, Effect of specimen size on interlaminar shear strength of unidirectional carbon fibre-epoxy, Compos. Eng. 4 (1994) 299–307, https://doi.org/10.1016/0961-9526(94)90080-9.

[49] M. Naebe, J. Wang, A. Amini, H. Khayyam, N. Hameed, L.H. Li, Y. Chen, B. Fox, Mechanical property and structure of covalent functionalised graphene/epoxy nanocomposites, Sci. Rep. 4 (2015), 4375, https://doi.org/10.1038/srep04375.

[50] L.-C. Tang, Y.-J. Wan, D. Yan, Y.-B. Pei, L. Zhao, Y.-B. Li, L.-B. Wu, J.-X. Jiang, G.-Q. Lai, The effect of graphene dispersion on the mechanical properties of graphene/epoxy composites, Carbon N. Y. 60 (2013) 16–27, https://doi.org/10.1016/J.CARBON.2013.03.050.

[51] K.A. Al-Shiblawi, V.F. Pershin, V.P. Jarcev, T.V. Pasko, Modification of epoxy resin using graphene, in: AIP Conf. Proc, AIP Publishing LLC, 2018, 020015, https://doi.org/10.1063/1.5079346.

[52] S.I. Abdullah, M.N.M. Ansari, Mechanical properties of graphene oxide (GO)/epoxy composites, HBRC J 11 (2015) 151–156, https://doi.org/10.1016/j.hbrcj.2014.06.001.

[53] G.J. Dvorak (Ed.), Inelastic Deformation of Composite Materials, Springer New York, New York, NY, 1991, https://doi.org/10.1007/978-1-4613-9109-8.

[54] S.R. Short, Characterization of interlaminar shear failures of graphite/epoxy composite materials, Composites 26 (1995) 431–449, https://doi.org/10.1016/0010-4361(95)90916-N.

[55] J. Qiu, C. Zhang, B. Wang, R. Liang, Carbon nanotube integrated multifunctional multiscale composites, Nanotechnology 18 (2007), 275708, https://doi.org/10.1088/0957-4484/18/27/275708.

[56] K. Bilisik, G. Erdogan, E. Sapanci, Interlaminar shear properties of nanostitched/nanoprepreg aramid/phenolic composites by short beam method, J. Compos. Mater. (2018), 002199831881152, https://doi.org/10.1177/0021998318811523.

[57] E.J. Garcia, B.L. Wardle, A. John Hart, Joining prepreg composite interfaces with aligned carbon nanotubes, Compos. Part A Appl. Sci. Manuf. 39 (2008) 1065–1070, https://doi.org/10.1016/J.COMPOSITESA.2008.03.011.

[58] J. Blanco, E.J. García, R. Guzmán de Villoria, B.L. Wardle, Limiting mechanisms of mode I interlaminar toughening of composites reinforced with aligned carbon nanotubes, J. Compos. Mater. 43 (2009) 825–841, https://doi.org/10.1177/0021998309102398.

[59] M.V. Hosur, U.K. Vaidya, C. Ulven, S. Jeelani, Performance of stitched/unstitched woven carbon/epoxy composites under high velocity impact loading, Compos. Struct. 64 (2004) 455–466, https://doi.org/10.1016/J.COMPSTRUCT.2003.09.046.

[60] H. Qian, A. Bismarck, E.S. Greenhalgh, M.S.P. Shaffer, Carbon nanotube grafted silica fibres: characterising the interface at the single fibre level, Compos. Sci. Technol. 70 (2010) 393–399, https://doi.org/10.1016/j.compscitech.2009.11.014.

[61] H.-S. Hwang, M.H. Malakooti, B.A. Patterson, H.A. Sodano, Increased interyarn friction through ZnO nanowire arrays grown on aramid fabric, Compos. Sci. Technol. 107 (2015) 75–81, https://doi.org/10.1016/J.COMPSCITECH.2014.12.001.

[62] Y. Gogotsi, J.A. Libera, M. Yoshimura, Hydrothermal synthesis of multiwall carbon nanotubes, J. Mater. Res. 15 (2000) 2591–2594, https://doi.org/10.1557/JMR.2000.0370.

[63] Ashok Bhatnagar, Lightweight Ballistic Composites, Elsevier, 2016, https://doi.org/10.1016/C2014-0-03657-X.

[64] P.S. Chua, Dynamic mechanical analysis studies of the interphase, Polym. Compos. 8 (1987) 308–313, https://doi.org/10.1002/pc.750080505.

[65] S. Mohanty, S.K. Verma, S.K. Nayak, Dynamic mechanical and thermal properties of MAPE treated jute/HDPE composites, Compos. Sci. Technol. 66 (2006) 538–547, https://doi.org/10.1016/J.COMPSCITECH.2005.06.014.